ELSEVIER

Journal of Photochemistry and Photobiology A: Chemistry 93 (1996) 119–128

Journal of PHOTOCHEMISTRY AND PHOTOBIOLOGY A: CHEMISTRY

Intramolecular and intermolecular photoinduced electron transfer in isomeric mesoporphyrin nitrobenzyl esters: structure and solvent effects ☆

Lluis Fajari [a], Pere Fors [b], Kamil Lang [b,1], Santiago Nonell [c], Francesc R. Trull [b,*]

[a] *Departament de Materials Orgànics Halogenats, CSIC, C/Jordi Girona 18, E-08034 Barcelona, Spain*

[b] *Departament de Química Orgànica, Facultat de Química, Universitat de Barcelona, C/Martí i Franquès 1, E-08028 Barcelona, Spain*

[c] *CETS Institut Químic de Sarrià, Universitat Ramon Llull, Via Augusta 390, E-08017 Barcelona, Catalonia, Spain*

Received 6 July 1995; accepted 11 August 1995

Abstract

Photoinduced intramolecular electron transfer was studied in a series of flexible dyads consisting of the isomeric *ortho*-, *meta*- and *para*-nitrobenzyl monoesters and diesters of mesoporphyrin existing preferentially in folded conformations. This process was compared with the intermolecular electron transfer between mesoporphyrin dimethyl ester and the 2-, 3- and 4-nitrobenzyl acetates. In both cases, electron transfer occurs from the porphyrin first excited singlet state, and the rate constant is lower in the ortho isomer, although intermolecular electron transfer is less isomer selective. The selectivity in the intermolecular case can be related to the isomer redox potentials, but in the dyads an ortho effect must also be taken into account; this effect produces a deviation from coplanarity between the nitro group and the phenyl ring. Electron paramagnetic resonance (EPR) in a low temperature matrix permits the charge transfer product to be detected. The process does not lead to the production of long-lived species, as shown by optoacoustic calorimetry. The efficiency of photoinduced electron transfer strongly depends on the ability of the solvent to stabilize the radical ion pair; this process occurs in CH_3OH, CH_3CN and CH_2Cl_2, but is inhibited in toluene and benzene. In the last two solvents, singlet oxygen is formed instead via energy transfer from the triplet state, with the same quantum yield as for the nitrobenzyl-free porphyrin.

Keywords: Photoinduced electron transfer; Porphyrins; Intramolecular; Donor–acceptor dyads

1. Introduction

Photoinduced electron transfer (PET) has been studied in intermolecular (collisional) and intramolecular donor–acceptor (D–A) systems, and its theoretical basis and experimental evidence have been extensively reviewed [1]. The understanding of these processes is important in the determination of the variables which influence the rate and efficiency of the light-harvesting process in bacteria and plants.

Provided that the molecular architecture and energy gap between the acceptor and donor are favourable, electron transfer may be observed [1b,2]. For a given D–A pair, the rate of PET depends on the acceptor-to-donor distance and orientation. Indeed, in rigid dyads, PET is found to decrease exponentially with increasing distance [1b,1d,3]. If, by contrast, the spacer tethering the chromophores is flexible, several suitable conformations are accessible depending on the presence of hindering substituents [4], the solvent and its polarity [5] and the temperature [6]; as a result, the system usually exhibits a more complex behaviour. By altering the relative spatial disposition of donor and acceptor, their electronic interactions (and PET) may be influenced. Eventually, large conformational changes can occur following PET [7].

Porphyrins are model compounds for chlorophylls, which are involved as electron donors in photosynthesis. They can be used to generate long-lived, charge-separated species, which originate from their first excited singlet state. As a consequence, a number of porphyrin-based supramolecules have been developed to model the primary photochemical step of photosynthesis [8]. For similar reasons, quinones have been the acceptors of choice accompanying porphyrin donors in many of these D–A model systems [5b,6b,8b–8d,8j,9]. Porphyrin dimers and trimers have also been employed as more complex D–A systems in which multistep electron transfer is used to stabilize the charge transfer state [8a,8f,8g,8j]. Other acceptors used include methylviologen (MV^{2+}) [5a], cyanine dyes [8i], pyromellitimide [10] and

☆ Dedicated to: the memory of the late Professors Fèlix Serratosa and Pedro J. Victory.

[1] On leave from the Institute of Inorganic Chemistry, Prague, Czech Republic.

* Corresponding author.

SSDI 1010-6030(95)04192-3

nitroaromatics [11]. As electron acceptors, nitroaromatics are interesting in that the free energy change for PET from a porphyrin is close to zero and therefore its sign can be reversed as a function of solvent or geometry.

In this paper, the PET behaviour of flexible dyads, consisting of a mesoporphyrin and one (or two) nitrobenzyl unit(s) (with the nitro group in the ortho, meta or para position) connected through the porphyrin propionate chain(s), is discussed. These dyads are monomeric models for porphyrin-containing photoconductive polymeric materials based on the principle of host–guest complexation driven by non-covalent interactions [12]. We have recently shown that they exist predominantly in folded conformations [13]. In this paper, we investigate the isomer and solvent dependence of the PET efficiency, the evolution of the charge transfer state and the photosensitization of singlet oxygen using (steady state and time-resolved) fluorescence spectroscopy, electron paramagnetic resonance (EPR), optoacoustic calorimetry and time-resolved near-IR phosphorescence detection.

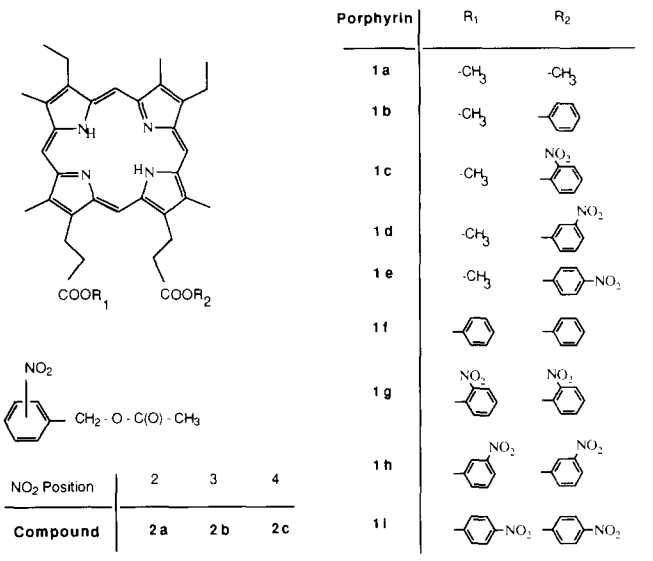

Scheme 1.

2. Experimental details

2.1. General

Due to the sensitivity of the compounds to light, sample manipulations were carried out in dim red light and under argon unless specified otherwise. The purity of all porphyrins was checked by thin layer chromatography (TLC) (silica gel; CH_2Cl_2–CH_3OH (10:1)) immediately before use and, when necessary, the samples were further purified by flash column chromatography. UV–visible spectra of approximately 1 μM solutions were recorded on a Perkin-Elmer Lambda 5 or a Shimadzu UV 2100 U spectrophotometer.

2.2. Materials

All solvents used in the steady state fluorescence and EPR measurements were of reagent grade quality, further purified by the usual procedures [14]. For all time-resolved fluorescence, optoacoustic calorimetry and $O_2(^1\Delta_g)$ phosphorescence experiments, solvents of spectroscopic or high performance liquid chromatography (HPLC) grade were used as received: CH_2Cl_2 was obtained from Merck (Uvasol) or distilled and dried over molecular sieves and toluene, acetonitrile and methanol were obtained from Panreac (Barcelona, Spain). 2,2,6,6-Tetramethylpiperidine (TEMP), 2,2,6,6-tetramethylpiperidine-1-oxyl (TEMPO) and 2-hydroxybenzophenone (2HBP) were obtained from Aldrich and were used without further purification. Tetra-*n*-butyl ammonium perchlorate (TBAP) was purchased from Fluka. The preparation of mesoporphyrin (MP) dimethyl ester (**1a**) [12c], MP dibenzyl ester (**1f**), MP nitrobenzyl monoesters (**1c–1e**) and MP nitrobenzyl diesters (**1g–1i**) [13] has been reported previously, as has the synthesis of *ortho*-, *meta*- and *para*-nitrobenzyl acetates [13] (see Scheme 1).

2.3. Relative fluorescence quantum yields Φ_f

The relative fluorescence quantum yields were determined with a Perkin-Elmer LS 50 spectrofluorometer using air-saturated benzene, CH_2Cl_2, CH_3CN and CH_3OH solutions of **1a–1i**. Emission spectra were recorded by exciting the maximum of the Soret band in each solvent: $\lambda_{exc} = 401$ nm (benzene), 399 nm (CH_2Cl_2), 393 nm (CH_3CN) and 394 nm (CH_3OH). Absorbances at λ_{exc} were optically matched in each solvent ($A \leqslant 0.1$; concentrations, 0.7 μM or less). Integration of the complete fluorescence spectrum and comparison with **1a** yielded Φ_f. The rate constants for the fluorescence quenching of **1a** (approximately 10 μM) by the nitrobenzyl acetates **2a–2c** (in the concentration range 0–0.1 M) in CH_2Cl_2 were derived in each case from conventional Stern–Volmer analysis. For each nitrobenzyl acetate, the quenching was explored at excitation wavelengths of 500, 531 and 566 nm (the porphyrin Q bands; in all cases the absorbance was less than 0.1) in order to prevent the direct excitation of the nitrobenzyl quenchers. All spectroscopic measurements were performed at room temperature.

2.4. Fluorescence kinetics

A picosecond, time-correlated, single-photon counting system was used to monitor the fluorescence decay kinetics. The excitation source was a frequency-doubled, mode-locked Coherent Antares 76s Nd:YAG laser coupled to a synchronously pumped, cavity-dumped dye laser emitting at 590 nm [11e]. The samples were dissolved in freshly distilled air-saturated dichloromethane or toluene. The absorbance was kept below 0.1. The fluorescence was detected at 620 nm.

2.5. EPR spectra

EPR spectra were recorded on a Varian 109 spectrometer. For the detection of the radical ion pair, a 500 W Oriel mer-

cury lamp was used. The photoproduced cation radical was measured in the frozen state (77 K) after degassing by four freeze–thaw cycles; 0.3 ml samples of 1 mM porphyrin (**1a**, **1e**) solutions in CH_2Cl_2 were used. The irradiation wavelength was above 440 nm (Oriel filter 59460 and solution filter consisting of 0.38 M $NiSO_4 \cdot 7H_2O$ and 0.07 M $CoSO_4 \cdot 7H_2O$ in 0.04 M aqueous H_2SO_4) to avoid any residual absorbance by the nitrobenzyl chromophore. For the study of singlet molecular oxygen production, optically matched porphyrin solutions (approximately 4 μM) were continuously irradiated above 330 nm (Oriel filter 59640) in the presence of 0.12 M TEMP in air-saturated benzene. The concentration of the reaction product, TEMPO, was estimated [15] from a calibration curve using the commercial product. At high TEMP concentrations, the rate equation for TEMPO formation is $[TEMPO] = I_a \Phi_\Delta \gamma_{AO2} t$, where I_a is the intensity of absorbed radiation, t is the irradiation time and γ_{AO2} is the efficiency of TEMP reaction with $^1O_2$, $\gamma_{AO2} = k_c/(k_p + k_c)$. Plotting [TEMPO] vs. irradiation time gives a straight line (zero-order kinetics), with a slope proportional to Φ_Δ.

2.6. Cyclic voltammetry measurements

Cyclic voltammetry measurements were performed in a three-electrode assembly using a Princeton Applied Research (PARC) 174A polarographic analyser, connected with a recorder (Philips PM-8133). The resistance was compensated via a polarographic interface AC 174150. A platinum spherical electrode (area, 12 mm^2) was used as the working electrode. The counter-electrode was a platinum wire of 0.8 mm diameter. The reference electrode was a KCl-saturated calomel electrode (SCE) separated from the bulk electrolyte by a fritted glass junction. All redox potentials of this work refer to this electrode. The concentrations of the compounds were 0.2–0.4 mM in CH_2Cl_2 containing 5×10^{-2} M TBAP as supporting electrolyte. The uncertainty in the peak potentials was ± 10 mV.

2.7. Laser-induced optoacoustic calorimetry (LIOAC)

The LIOAC set-up and data treatment procedures used to derive calorimetric and kinetic information are identical to those described in the literature [16]. An N_2 laser (Radiant Dyes Laser Accessories GmbH, Warmelskirchen, Germany), delivering 6 ns pulses, was used to excite samples contained in a quartz cuvette (path length, 1 cm). The diameter of the beam in the cuvette was reduced to about 1 mm by a 100 cm lens/1 mm aperture combination. The laser fluence was varied using a set of neutral density filters. The amplitude of the first signal maximum H was taken to be proportional to the heat emitted in the fast radiationless deactivation processes. The absorbance at the excitation wavelength of 337 nm was varied from approximately 0.070 to 0.345 for all MP esters assayed (**1a** and **1g–1i**) and 2HBP, the calorimetric reference used. As **1a** and **1g–1i** are difficult to dissolve in neat CH_3OH, solutions were prepared by dissolving each porphyrin in a few drops of CH_2Cl_2, diluting with CH_3OH and separating any non-dissolved solid on a 0.2 μm membrane filter.

2.8. Time-resolved singlet oxygen phosphorescence

The apparatus used to monitor the $O_2(^1\Delta_g)$ phosphorescence decay kinetics is essentially identical to the LIOAC spectrometer (above) except for the detection system. The luminescence arising from the cuvette was passed through a 1050 nm cut-off silicon filter and a 1270 nm interference filter, and detected with a 5 mm diameter Judson J16 5Sp germanium diode. The zero-time signal intensity was taken as a measure of the initial $O_2(^1\Delta_g)$ concentration. Details of the apparatus and data handling procedures have been given elsewhere [17]

3. Results and discussion

3.1. Ground state properties. Geometries

We have recently shown, mainly on the basis of proton nuclear magnetic resonance (^{1}H-NMR) results, that the MP nitrobenzyl monoesters **1c–1e** and diesters **1g–1i** occur largely in a folded conformation (Fig. 1, bottom) in $CDCl_3$ and even more so in C_6D_6 [12]. This conformation is stabilized by π–π interactions between the porphyrin and nitrobenzyl halves [18]. Theoretical calculations confirm this geometry and predict nearly coplanar nitro and phenyl groups in the m and p isomers of the dyads, as well as in the three isomers of the nitrobenzyl acetates (**2a–2c**), but a dihedral angle close to 40° in the ortho isomers **1c** and **1g** [13].

The absorption spectra of **1c–1e** and **1g–1i** show minor differences with respect to the simple sum of the spectra of the MP chromophore (i.e. **1a**) plus the respective 2-, 3- or 4-nitrobenzyl acetates (**2a–2c**). A slight red shift (1–4 nm) in the position of the Soret band (but not of the Q bands) of the dyads and a concomitant broadening (3–8 nm at half-maximum) can be observed for the three isomers. These effects are moderately solvent dependent (Table 1), with the

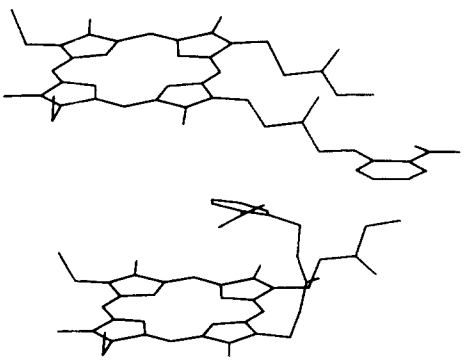

Fig. 1. AM1 geometries for **1c** in its extended (top) and folded (bottom) conformations. In the folded conformation of **1g–1i**, each propionate chain is folded towards opposite sides of the porphyrin plane.

Table 1
Position (λ_{max}, nm) and intensity (log ϵ, M^{-1} cm^{-1}, in parentheses) of the UV–visible absorption bands of the mesoporphyrin nitrobenzyl monoesters **1c–1e** in different solvents [a]

Solvent	Soret	IV	III	II	I
Benzene	401 (5.14±0.02)	498–499 (4.12±0.02)	530–531 (3.94±0.01)	569 (3.80±0.01)	622–623 (3.69±0.01)
CH_2Cl_2	398–399 (5.16±0.03)	497 (4.12±0.02)	531–532 (3.97±0.02)	566–567 (3.82±0.02)	620 (3.65±0.02)
CH_3OH	393–394 (5.18±0.03)	496–497 (4.14±0.02)	529–530 (4.00±0.03)	566–567 (3.84±0.03)	618±619 (3.67±0.02)

[a] Values of λ_{max} (nm) (log ϵ, M^{-1} cm^{-1}) for **1a**: in benzene, 400 (5.19), 498 (4.15), 531 (3.98), 569 (3.81), 623 (3.73); in CH_2Cl_2, 399 (5.12), 498 (4.04), 533 (3.89), 567 (3.72), 620 (3.59); in CH_3OH + 1% DMSO, 390 (5.15), 495 (4.07), 529 (3.91), 566 (3.73), 618 (3.59).

largest differences being observed in methanol and the largest band broadening in benzene. These weak perturbations indicate a correspondingly small degree of π-system distortion.

In the absorption spectra of mixtures of the MP dimethyl ester (**1a**) and an excess of any of the 2-, 3- or 4-nitrobenzyl acetates (**2a–2c**), overlap of the porphyrin Soret band with the more intense absorption due to nitrobenzyl precludes the observation of analogous changes and therefore of any degree of π-system distortion.

3.2. Excited state properties

3.2.1. Fluorescence spectra and yields in the linked systems

The fluorescence emission spectra of **1c–1e** and **1g–1i** in $CHCl_3$, CH_2Cl_2, CH_3CN and CH_3OH have the same shape as that of the dimethyl ester **1a**, with a maximum at 621–623 nm. In benzene, a small bathochromic shift to 625 nm occurs, but no new bands are observed. The excitation spectra are also basically identical in all cases and equal to the respective absorption spectra. These observations indicate that no significant alteration of the first excited singlet state vs. ground state geometry of the porphyrin skeleton occurs in the dyads relative to **1a**.

Table 2
Relative fluorescence quantum yields, fluorescence lifetimes and PET rate constants in air-saturated CH_2Cl_2 for the model porphyrins **1a** and **1f**, dyads **1c–1e** and triads **1g–1i**

Porphyrin	Φ_f [a]	τ_f [b] (ns)	k_{ET}^{TR} [c] ($\times 10^8$ s^{-1})	k_{ET}^{SS} [d] ($\times 10^8$ s^{-1})
1a	1	10.3	–	–
1c	0.58	6.7	0.55	0.68
1d	0.31	3.2	2.2	2.1
1e	0.33	3.4	2.0	1.9
1f	0.96	10.9	–	–
1g	0.42	5.7	0.8	1.3
1h	0.18	1.9	4.4	4.3
1i	0.20	2.1	3.8	3.8

[a] From steady state fluorescence; relative to **1a**; errors ±10%; samples of $Abs^{399} = 0.1$; $\lambda_{exc} = 399$ nm.
[b] From time-resolved fluorescence (same solvent and concentration; $\lambda_{exc} = 570–590$ nm; $\lambda_{det} = 620$ nm).
[c] From fluorescence decay.
[d] From fluorescence spectra with $\tau^0 = 10.5$ ns.

The fluorescence quantum yields Φ_f (relative to **1a**) for **1c–1e** and **1g–1i** in air-saturated CH_2Cl_2 are shown in Table 2. The two nitro-free porphyrins (**1a**, **1f**) show the same Φ_f value (no effect by the benzyl groups), whereas the presence of a nitro group on the phenyl ring decreases Φ_f, indicating an additional fast deactivation process. This is identified as a PET process originating from the donor first excited singlet state, by analogy with similar observations in related porphyrin–(poly)nitrobenzene [5b,9c,11,12d] and porphyrin–quinone [3a,5b,6b,8b–8d,8j,9] dyads.

As expected, the decrease in the Φ_f values is larger in the porphyrins substituted by two nitrobenzyl residues. For the monosubstituted and disubstituted compounds, Φ_f is isomer dependent, with the 3- and 4-nitrobenzyl isomers showing similar Φ_f values which are clearly lower than those of the 2-nitrobenzyl derivatives. This corresponds to a more efficient PET process in the 3- and 4-nitrobenzyl isomers, a behaviour that correlates with the different (relative to the 2-nitrobenzyl isomer) nitro-to-phenyl orientation theoretically calculated for both of these compounds in their folded conformation [13].

A deeper insight into the electron transfer kinetics can be obtained from the fluorescence decay data (Fig. 2 and Table 2). All compounds show strictly monoexponential decay, indicating that the conformations of the dyads equilibrate within the singlet state lifetime of the donor porphyrin. A mean lifetime of 10.6±0.3 ns was found for the models **1a** and **1f**, while the lifetimes of the dyads depend on the number of mononitrobenzyl acceptors and the nitro group position. Assuming an equal radiative lifetime for all porphyrins [5b], the rate constants for electron transfer k_{ET} were calculated using the equation $k_{ET}^{TR} = 1/\tau_f - 1/\tau_f^{1a}$, where τ_f^{1a} and τ_f are the fluorescence lifetimes of **1a** and the linked systems respectively. k_{ET} values were also obtained from the steady state fluorescence data, using the equation $k_{ET}^{SS} = (1 - \Phi_f)/\tau_f^{1a}\Phi_f$. The values resulting from the two procedures are similar (Table 2).

For all dyads (i.e. **1c–1e**, **1g–1i**), the electron transfer rate constants are approximately equal for the 3- and 4-nitroben-

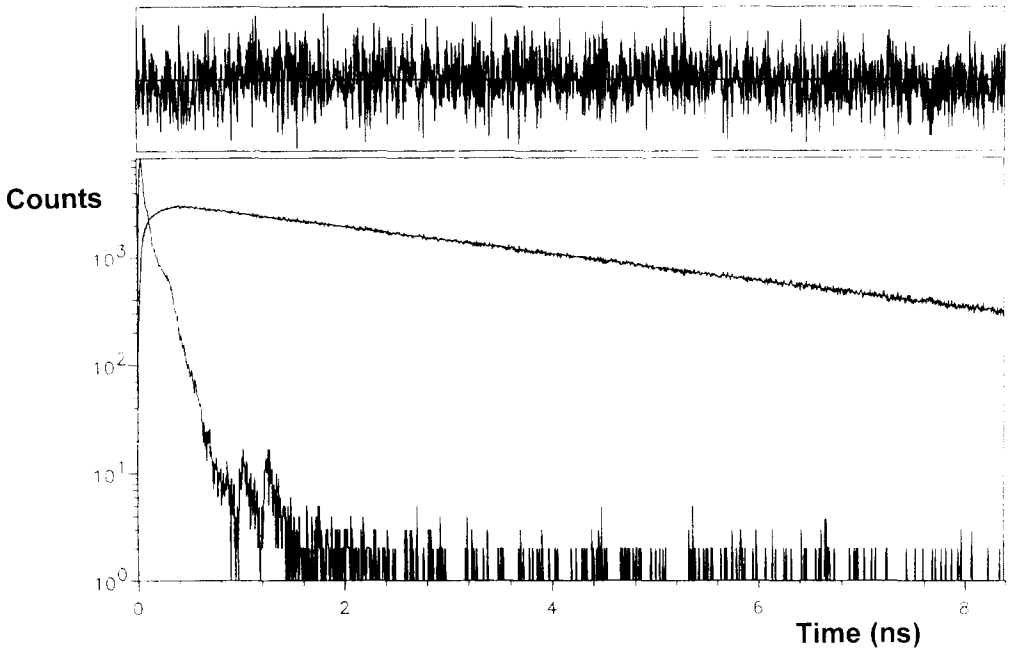

Fig. 2. Fluorescence decay of **1e** in air-saturated CH_2Cl_2 and residuals of the fit. $\lambda_{exc} = 570$ nm; $\lambda_{obs} = 620$ nm; $\tau = 3.39$ ns; $\chi^2 = 1.209$. Use of a biexponential function did not improve the fit significantly ($\chi^2 = 1.188$).

zyl esters, but about one-third of this value for the 2-nitrobenzyl esters. For the diesters, the rate constants k_{ET} are roughly twofold larger than those of the monoesters; apparently, the two nitrobenzyl residues of these systems behave as two independent units bound to the same porphyrin (i.e. triads).

The electron transfer kinetics of these dyads are strongly influenced by the solvent polarity (Table 3). In benzene, the Φ_f values for **1g–1i** are the same as that of **1a**, and in aerated toluene the lifetimes of **1a** and **1c** are 11.9 ns and 12.6 ns respectively. Clearly, electron transfer is inhibited in the two solvents. In contrast, in methanol, the relative Φ_f values for **1g–1i** are smaller than those in CH_2Cl_2, corresponding to more efficient electron transfer in the more polar solvent. The values in acetonitrile are comparable with those in CH_2Cl_2.

The rate constants k_{ET} deduced for **1g–1i** in CH_3CN are comparable with those in CH_2Cl_2, whereas in CH_3OH they are 3–6 times higher (Table 3). The behaviour in acetonitrile is irregular: although this is a more polar solvent than methanol, PET is clearly less effective. We offer no explanation for this, although similar solvent effects have been reported for intermolecular electron transfer processes to nitrobenzenes [19]. However, the general trend shown by Table 3 is that PET efficiency in our dyads increases with solvent polarity.

Table 3
Solvent dependence of the relative fluorescence quantum yields and PET rate constants for **1a** and porphyrin triads **1g–1i**[a]

Porphyrin	CH_2Cl_2		Benzene		CH_3CN		CH_3OH	
	Φ_f	k_{ET}	Φ_f	k_{ET}	Φ_f	k_{ET}	Φ_f	k_{ET}
1a	1.00	–	1.00	–	1.00	–	1.00	–
1g	0.42	0.8	1.01	–	0.40	1.1	0.11	5.9
1h	0.18	4.4	0.95	–	0.25	0.7	0.05	4.2
1i	0.20	3.8	0.98	–	0.14	1.5	0.09	2.5

[a] In all solvents, the value for **1a** is arbitrarily taken as 1.00.

3.2.2. *Intermolecular fluorescence quenching*

Intermolecular PET from MP dimethyl ester (**1a**) to the isomeric nitrobenzyl acetates (**2a–2c**) was investigated by steady state fluorescence quenching in air-saturated CH_2Cl_2.

Formation of a ground state non-fluorescent complex (static quenching) can be ruled out since the Stern–Volmer plot is linear [20], despite the large excess of quencher (**2a–2c**) relative to **1a**. Dynamic (collisional) quenching is therefore responsible for the overall quenching process.

From the slope of the Stern–Volmer plots ($K_{SV} = 5.5 \pm 0.5$, 9.5 ± 0.3 and 11.1 ± 0.4 for **2a**, **2b** and **2c** respectively) and the lifetime of the model systems (10.6 ns, cf. Table 2), the corresponding bimolecular electron transfer rate constants k_q have been calculated as 5.2×10^8, 9.0×10^8 and 10.2×10^8 $M^{-1}\ s^{-1}$. These k_q values indicate that intermolecular PET from porphyrin to nitrobenzyl is approximately equally efficient for 3- and 4-nitrobenzyl acetates (**2b** and **2c**) but less efficient for 2-nitrobenzyl acetate (**2a**), in agreement with the results for the (intramolecular) dyads, although the ratio of the efficiencies is smaller (1.8 vs. 3 in the dyads); hence intermolecular PET is less isomer discriminating than intramolecular PET. This difference in behaviour correlates with the distinct NO_2-to-phenyl dihedral angles calculated [13] for the folded *ortho*-dyad **1c** (40°) and *ortho*-acetate **2a** (9°).

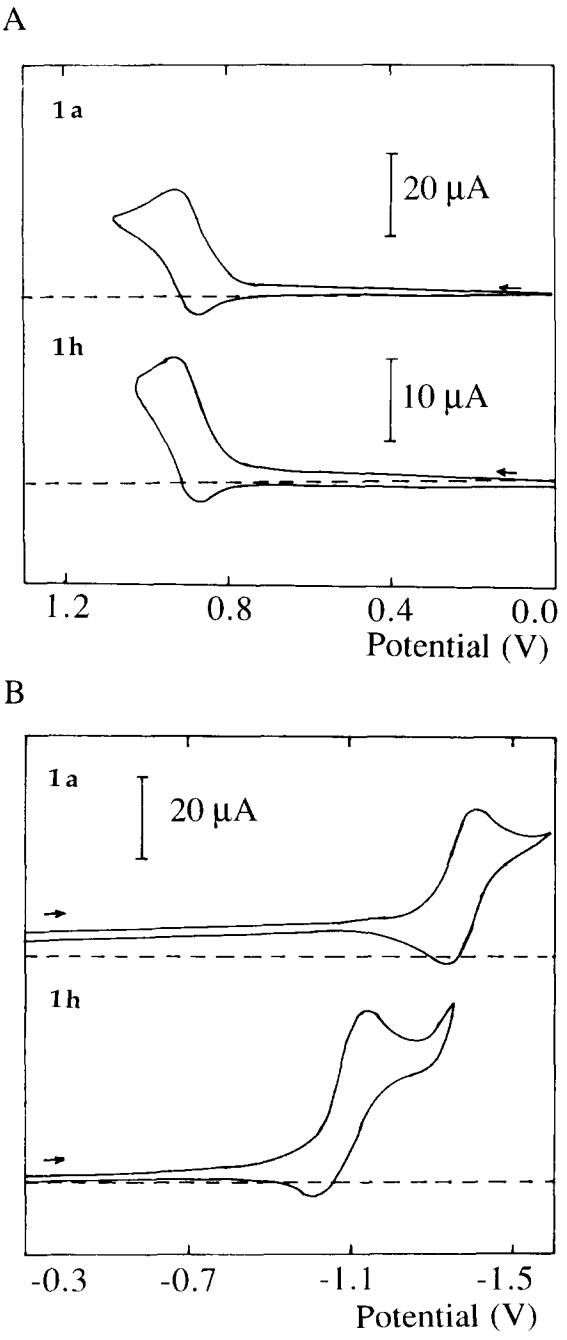

Fig. 3. (A) Cyclic voltammograms corresponding to the oxidation of **1a** and **1h**. Scan rate, 0.1 V s^{-1}; 5×10^{-2} M TBAP in CH_2Cl_2; potentials vs. SCE. (B) Cyclic voltammograms corresponding to the reduction of **1a** and **1h** under identical conditions as for oxidation.

3.2.3. EPR evidence for radical ion pair formation

Additional evidence for a deactivation mechanism involving PET was obtained from EPR spectroscopy. On continuous irradiation of **1a** in a frozen solution in CH_2Cl_2, the porphyrin cation radical single-line EPR signal [9a,9c,9h] gradually increases with $g = 2.0019$ and a peak-to-peak linewidth $\Delta H_{pp} \approx 0.5$ mT. After warming to room temperature and freezing again, this signal disappears. On the other hand, very low intensities of porphyrin cation radical signals were observed for **1a** in the presence of 0.1 M (approximately 100-fold excess) nitrobenzene, and for the dyad **1e**. In these cases, rapid back electron transfer from the initially formed charge transfer intermediate decreases the steady state concentration of the radicals.

3.3. Cyclic voltammetry

The standard electrode potentials allow the estimation of the energy of the charge transfer state. Fig. 3 shows the voltammograms of **1h** and the reference donor **1a**. The shapes of the voltammograms of all other dyads of this work, i.e. **1c–1e**, **1g** and **1i**, are similar.

1a undergoes two reversible electrode processes, which can be attributed to the one-electron oxidation and reduction of the porphyrin core [21]. Oxidation is characterized by the anodic peak potential $E_{pa}^{ox} = 0.92$ V ($E_{pa}^{ox} - E_{pc}^{ox} = 60$–$65$ mV, for 0.05, 0.1 and 0.2 V s^{-1}). Reduction occurs at a cathodic peak potential of -1.41 V. For the dyads, oxidation is also reversible and has the same E_{pa}^{ox} as **1a**; reduction of the porphyrin nucleus is still observed at about -1.43 V, but an additional quasi-reversible reduction process ($E_{pa}^{red} - E_{pc}^{red} = 100$ mV, for 0.1 V s^{-1}) is observed near -1.1 V (cf. Fig. 3; the precise value depends on the isomer, see Table 4). The peak current i_{pc}^{red} of this process is the same for **1c–1e**, and equal to i_{pa}^{ox} for the oxidation of the porphyrin nucleus. In **1g–1i**, i_{pc}^{red} is twice as high, consistent with the involvement of two electrons in these compounds. We con-

Table 4
Standard redox potentials [a] ($E^{\circ}_{(D^+/D)}$ and $E^{\circ}_{(A/A^-)}$), non coulombic contribution to ΔG°_{ET} [b] (ΔG°_{NC}) and electron transfer free energy change [c] (ΔG°_{ET}) for systems **1a–2a**, **1a–2b**, **1a–2c**, dyads **1c–1e** and triads **1g–1i** in CH_2Cl_2

System	$E^{\circ}_{(D^+/D)}$ (V)	$E^{\circ}_{(A/A^-)}$ (V)	ΔG°_{NC} (eV)	ΔG°_{ET} (eV)
1a–2a	0.89 [d]	−1.01 [e]	−0.10	−0.26
1a–2b	0.89 [d]	−0.98 [f]	−0.13	−0.29
1a–2c	0.89 [d]	−0.98 [g]	−0.13	−0.29
1c	0.90	−1.13	0.03	−0.24
1d	0.90	−1.08	−0.02	−0.29
1e	0.90	−1.09	−0.01	−0.28
1g	0.91	−1.12	0.03	−0.24
1h	0.90	−1.09	−0.01	−0.28
1i	0.91	−1.08	−0.01	−0.28

[a] Assumed to be equal to half-wave potentials $E_{1/2}$. These are derived from the cyclic voltammetry measured peak potentials E_{pa} and E_{pc}; error limit, ±0.01 V; $E_{1/2}^{ox}$ is taken to be 28 mV more negative than E_{pa}^{ox}; $E_{1/2}^{red}$ is taken to be 40 mV more positive than E_{pc}^{red}.
[b] $\Delta G^{\circ}_{NC} = E^{\circ}_{(D^+/D)} - E^{\circ}_{(A/A^-)} - E_{0,0}$; error limit, ±0.02 eV. The values for **2a–2c** are for electron transfer from **1a**, with $r_{DA} = 10$ Å. The values for **1c–1i** are calculated assuming $r_{DA} = 6$ Å (folded conformation).
[c] $\Delta G^{\circ}_{ET} = \Delta G^{\circ}_{NC} - e/4\pi\epsilon_0 \times 1/\epsilon r_{DA}$; error limit, ±0.02 eV; $e/4\pi\epsilon_0 \times 1/\epsilon r_{DA}$ is 0.16 eV for $r_{DA} = 10$ Å and 0.27 eV for $r_{DA} = 6$ Å.
[d] Corresponds to **1a**.
[e] Corresponds to **2a**.
[f] Corresponds to **2b**.
[g] Corresponds to **2c**.

clude that the new process is the reduction of the nitrobenzyl group(s).

The standard redox potentials $E^{\circ}_{(D^+/D)}$ and $E^{\circ}_{(A/A^-)}$ for both the linked systems and the nitrobenzyl acetates, calculated from the experimental half-wave potentials [22], are shown in Table 4.

The $E^{\circ}_{(A/A^-)}$ values of dyads **1c–1e** and triads **1g–1i** are similar. For all isomers, the reduction potential of the nitrobenzyl group in the acetate series is approximately 110 mV more positive than in the corresponding linked systems. This difference reflects the existence of D–A interactions in the dyads, further confirming the predominance of folded forms. Within each series of compounds, the reduction potential of the *ortho*-nitro isomer (**1c**, **1g** and **2a**) is more negative than that of the meta and para counterparts (40–50 mV for **1c** and **1g**, but only 30 mV for **2a**). This probably reflects the different orientation of the nitro group for the ortho isomers (see above).

3.4. Energetics of PET in different solvents

The driving force ΔG°_{ET} for PET in each of the extreme conformations available to the present systems can be estimated from the standard redox potentials of the donor (D) and acceptor (A), the MP(S_1) energy ($E_{0,0}=2$ eV) [23] and the theoretically calculated geometries [13], using the Rehm–Weller equation [1a,24].

For the present dyads, the contribution to ΔG°_{ET} of the non-coulombic terms is nearly zero in CH_2Cl_2 (Table 4). Therefore the exergonicity of PET must be provided by the ion pair coulombic stabilizing contribution, and this in turn is related to the r_{DA} value and to the solvent static dielectric constant ϵ_r. A limiting ΔG°_{ET} value for the folded conformation can be estimated using the theoretically calculated geometry, with a CTC distance of approximately 6 Å for all isomers [13]. The values of ΔG°_{ET} thus obtained (Table 4) clearly indicate that, in CH_2Cl_2, the process is thermodynamically feasible for all isomers, in agreement with the experimental observations.

If an analogous estimation is made for the extended conformation in the theoretically calculated geometry [13], with a CTC distance of 12 Å, ion pair stabilization no longer results in negative ΔG°_{ET} values. Thus PET ought to be observed in the dyads only from folded conformations.

For the intermolecular systems, the results are comparable (Table 4). Non-coulombic terms result in negative ΔG°_{ET} values, which allows for electron transfer at contact pair distances of approximately 10 Å, based on the bond lengths and geometries from the literature [25]. As for the extended dyads, coulombic stabilization is negligible.

The values of ΔG°_{ET} for the intermolecular PET process (i.e. from **1a** to **2a–2c**) and for intramolecular PET in dyads **1c–1e** and triads **1g–1i** in benzene, CH_3CN and CH_3OH, obtained using the complete Rehm–Weller equation [26] assuming in all cases the same geometries as in CH_2Cl_2, are shown in Table 5.

Table 5
PET free energy change ($\Delta G^{\circ}_{ET}(\epsilon)$) for systems **1a–2a**, **1a–2b**, **1a–2c**, dyads **1c–1e** and triads **1g–1i** in solvents of different dielectric constant

System	r_{DA} (Å)	$\Delta G^{\circ}_{ET}(\epsilon)$ (eV) [a]		
		Benzene ($\epsilon_r=2.38$)	CH_3CN ($\epsilon_r=35.94$)	CH_3OH ($\epsilon_r=32.66$)
1a–2a	10	0.35	−0.43	−0.42
1a–2b	10	0.32	−0.46	−0.45
1a–2c	10	0.32	−0.46	−0.45
1c	6	0.03	−0.38	−0.37
1d	6	−0.02	−0.43	−0.42
1e	6	−0.01	−0.42	−0.41
1g	6	0.03	−0.38	−0.37
1h	6	−0.01	−0.42	−0.41
1i	6	−0.01	−0.42	−0.41

[a] Calculated from $\Delta G^{\circ}_{ET}(CH_3Cl_2)$ using the equation: $\Delta G^{\circ}_{ET}(\epsilon)=\Delta G^{\circ}_{ET}(CH_2Cl_2)+e/4\pi\epsilon_0\times(1/2r_D+1/2r_A-1/r_{DA})\times(1/\epsilon_r-1/\epsilon_r^{CH_2Cl_2})$.

In benzene, PET has a nearly zero driving force for the dyads and a positive value for the unbound systems, in agreement with the experimental observation of the absence of electron transfer. Although in this solvent the dyads adopt a geometry presumably at least as favourable for electron transfer as that in CH_2Cl_2 [13], this is clearly overcompensated by the destabilizing solvent contribution to ΔG°_{ET}. An analogous behaviour has been reported for chlorophyll–porphyrin dyads [27].

In CH_3OH and CH_3CN, ΔG°_{ET} values more negative than in CH_2Cl_2 are obtained, as expected. This is in agreement with the larger experimental electron transfer rate constants observed in methanol (Table 3) but, as noted above, conflicts with the values obtained in acetonitrile.

3.5. Kinetics of PET

The rate constant of non-adiabatic electron transfer is related to electronic κ_{el} and nuclear κ_n factors [1c,1d,24,28]. The electronic factor is mainly influenced by the electronic coupling energy, which decreases exponentially with increasing separation distance r_{DA} and also depends on the relative D–A orientation. The nuclear factor is an exponential term which involves the structural displacement in the reactants and surrounding solvent molecules on electron transfer. It contains contributions from the driving force of the reaction ΔG°_{ET} and the reorganization energy λ. The latter is divided into a solvent-independent term λ_{in}, which is relatively small (0.1–0.3 eV) for large molecules such as porphyrins [29], and the solvent reorganization energy λ_{out}, which is related to the D–A geometry.

For the intermolecular processes, the assumption that diffusional separation of the encounter pair is much faster than electron transfer predicts that k_{ET} is proportional to the observed quenching rate constant k_q through the equilibrium constant for the formation of the encounter pair, which is assumed to be the same for the three isomers [24,30]. This

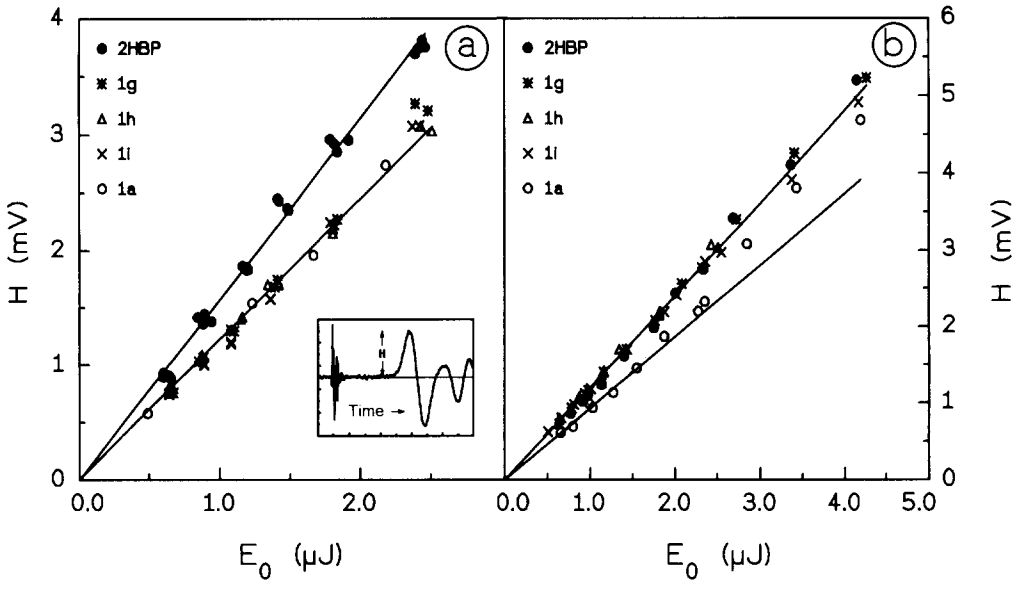

Fig. 4. Laser energy dependence of the optoacoustic signal for **1a**, **1g–1i** and 2HBP: (a) in air-saturated toluene; absorbances were matched at 0.107 ± 0.002; inset: optoacoustic signal for 2HBP at $E_0 = 2.43$ μJ; (b) in air-saturated methanol; absorbances were matched at 0.140 ± 0.002. For **1a**, the deviations from linearity at high laser energies should be noted.

allows a comparison of the ratios of calculated κ_n and experimental k_q for the pairs **1a**–(**2a–2c**).

Using the same geometry estimated above ($r_{DA} = 10$ Å) for the three isomeric contact pairs, the resulting ratio of the nuclear factors for the quenching of **1a** by **2b** and **2c** relative to **2a** is about 1.5. This is close to the experimental ratio (1.8) of the quenching rate constants. The differences in intermolecular electron transfer efficiency between **2a**, **2b** and **2c** thus appear to be due mainly to the nuclear factor κ_n.

For the covalently bound D–A systems, an approximate estimation can be performed using the geometry calculated theoretically for the folded conformation model ($r_{DA} = 6$ Å). Theoretical calculations show that the largest differences between the isomers occur in their folded conformations, namely the large deviation from planarity of the *ortho*-nitro group with respect to the phenyl ring (40°), which is not found for the meta and para counterparts. Hence choosing this conformation for the κ_n and κ_{el} calculations should produce the largest ratio among the three isomers. The resulting ratio of the nuclear factors for **1d** and **1e** relative to **1c** is about 1.7, while the ratio of the experimental k_{ET} values is 3. In this case, the nuclear factor alone cannot account for the ratio of the experimentally observed PET rates; the electronic factor and, more specifically, the D–A electronic coupling must play a significant role [5b]. This is consistent with the distinct nitro-to-phenyl dihedral angle, resulting in a different porphyrin-to-nitro group orientation in the ortho relative to the meta and para isomers.

3.6. Fate of the charge transfer state. LIOAC studies

The laser energy dependence of the LIOAC amplitude for **1g–1i**, **1a** and 2HBP in air-saturated toluene is shown in Fig. 4(a). The behaviour is the same for the three dyads and for the model compound **1a**, giving an average value of α, the fraction of absorbed energy released as fast heat, of 0.78 ± 0.06. Hence the dyads behave as the model compound **1a**, i.e. total suppression of PET in this solvent and concomitant singlet oxygen production (see below). The α value indicates approximately 20% energy storage, consistent with the reported value for the singlet oxygen quantum yield $\Phi_\Delta = 0.57$ [31].

Fig. 4(b) shows the results of similar experiments in air-saturated methanol. In this case, the behaviour of the three nitrobenzyl isomers **1g–1i** is very different from that of **1a**, but indistinguishable from that of 2HBP. Thus $\alpha = 1.00 \pm 0.05$ must be assigned to the three isomers, indicating that all absorbed energy is rapidly dissipated as heat through a quantitative electron transfer step followed by fast charge recombination leading to ground state products. Thus intramolecular electron transfer effectively suppresses the singlet oxygen sensitization ability of the present porphyrin dyads in polar media, whilst it is left intact in non-polar environments.

Acknowledgements

This work was part of the CICYT research programme MAT91-0901-C03-01. Financial support to P.F. and K.L. from the Spanish Ministerio de Educación y Ciencia is acknowledged. S.N. thanks the Max-Planck-Gesellschaft for an Otto Hahn fellowship. Credit should be given to Dr. J. DeGraziano and Professors D. Gust and T.A. Moore (Center for the Study of Early Events in Photosynthesis, Arizona State University) for their assistance with the time-resolved fluo-

rescence experiments. Thanks are due to Professor J. Claret (University of Barcelona) for assistance with the electrochemical measurements and to Professor S.E. Braslavsky (MPI für Strahlenchemie, Mülheim/Rühr, Germany) for comments and encouragement.

References

[1] (a) M. Chanon, M.D. Hawley and M.A. Fox, in M.A. Fox and M. Chanon (eds.), *Photoinduced Electron Transfer*, Elsevier Science Publishers, Amsterdam, 1988, Part A, pp. 1–59. (b) M.R. Wasielewski, in M.A. Fox and M. Chanon (eds.), *Photoinduced Electron Transfer*, Elsevier Science Publishers, Amsterdam, 1988, Part A, pp. 161–206. (c) J.R. Bolton and M.D. Archer, in R. Bolton, N. Mataga and G. McLendon (eds.), *Electron Transfer in Inorganic, Organic, and Biological Systems*, Advances in Chemistry Series 228, ACS, Washington, 1991, pp. 7–23. (d) N. Sutin, in R. Bolton, N. Mataga and G. McLendon (eds.), *Electron Transfer in Inorganic, Organic, and Biological Systems*, Advances in Chemistry Series 228, ACS, Washington, 1991, pp. 25–43.

[2] (a) F.D. Lewis and E.L. Burch, *J. Am. Chem. Soc., 116* (1994) 1159–1160. (b) P. Jacques and X. Allonas, *J. Photochem. Photobiol. A: Chem., 78* (1994) 1–5.

[3] (a) M.R. Wasielewski and M.P. Niemczyk, *J. Am. Chem. Soc., 106* (1984) 5043–5045. (b) H. Oevering, M.N. Paddon-Row, M. Heppener, A.M. Oliver, E. Cotsaris, J.W. Verhoeven and N.S. Hush, *J. Am. Chem. Soc., 109* (1987) 3258–3269.

[4] A. Osuka, K. Maruyama and S. Hirayama, *Tetrahedron, 45* (1989) 4815–4829.

[5] (a) Y. Kanda, H. Sato, T. Okada and N. Mataga, *Chem. Phys. Lett., 129* (1986) 306–309. (b) J. Liu, J.A. Schmidt and J.R. Bolton, *J. Phys. Chem., 95* (1991) 6924–6927.

[6] (a) C.A. Berg-Brennan, D.I. Yoon and J.T. Hupp, *J. Am. Chem. Soc., 115* (1993) 2048–2049. (b) L.R. Khundkar, J.W. Perry, J.E. Hanson and P.B. Dervan, *J. Am. Chem. Soc., 116* (1994) 9700–9709.

[7] A.M. Brouwer, R.D. Mout, P.H. Maassen van den Brink, H.J. van Ramesdonk, J.W. Verhoeven, S.A. Jonker and J.M. Warman, *Chem. Phys. Lett., 186* (1991) 481–489.

[8] (a) R.R. Bucks, T.L. Netzel, I. Fujita and S.G. Boxer, *J. Phys. Chem., 86* (1982) 1947–1955. (b) T.A. Moore, D. Gust, P. Mathis, J.-C. Mialocq, C. Chachaty, R.V. Bensasson, E.J. Land, D. Doirit, P.A. Liddell, W.R. Lehman, G.A. Nemeth and A.L. Moore, *Nature, 307* (1984) 630–632. (c) D. Gust, T.A. Moore, L.R. Makings, P.A. Liddell, G.A. Nemeth and A.L. Moore, *J. Am. Chem. Soc., 108* (1986) 8028–8031. (d) D. Gust, T.A. Moore, P.A. Liddell, G.A. Nemeth, L.R. Makings, A.L. Moore, D. Barrett, P.J. Pessiki, R.V. Bensasson, M. Rougée, C. Chachaty, F.C. De Schryver, M. Van der Auweraer, A.R. Holzwarth and J.S. Connolly, *J. Am. Chem. Soc., 109* (1987) 846–856. (e) R.M. Hermant, P.A. Liddell, S. Lin, R.G. Alden, H.K. Kang, A.L. Moore, T.A. Moore and D. Gust, *J. Am. Chem. Soc., 115* (1993) 2080–2081. (f) J.-C. Chambron, A. Harriman, V. Heitz and J.-P. Sauvage, *J. Am. Chem. Soc., 115* (1993) 6109–6114. (g) J.-C. Chambron, A. Harriman, V. Heitz and J.-P. Sauvage, *J. Am. Chem. Soc., 115* (1993) 7419–7425. (h) S. Prathapan, T.E. Johnson and J.S. Lindsey, *J. Am. Chem. Soc., 115* (1993) 7519–7520. (i) J.S. Lindsey, P.A. Brown and D.A. Siesel, *Tetrahedron, 45* (1989) 4845–4866. (j) M.R. Wasielewski, *Chem. Rev., 92* (1992) 435–461.

[9] (a) A.R. McIntosh, A. Siemiarczuk, J.R. Bolton, M.J. Stillman, T.-F. Ho and A.C. Weedon, *J. Am. Chem. Soc., 105* (1983) 7215–7223. (b) A. Siemiarczuk, A.R. McIntosh, T.-F. Ho, M.J. Stillman, K.J. Roach, A.C. Weedon, J.R. Bolton and J.S. Connolly, *J. Am. Chem. Soc., 105* (1983) 7224–7230. (c) M.C. González, A.R. McIntosh, J.R. Bolton and A.C. Weedon, *J. Chem. Soc., Chem. Commun.*, (1984) 1138–1140. (d) J.R. Bolton, T.-F. Ho, S. Liauw, A. Siemiarczuk, C.S.K. Wan and A.C. Weedon, *J. Chem. Soc., Chem. Commun.*, (1985) 559–560. (e) A. Osuka, S. Morikawa, K. Maruyama, S. Hirayama and T. Minami, *J. Chem. Soc., Chem. Commun.*, (1987) 359–361. (f) Y. Aoyama, M. Asakawa, Y. Matsui and H. Ogoshi, *J. Am. Chem. Soc., 113* (1991) 6233–6240. (g) T. Hayashi, T. Miyahara, N. Hashizume and H. Ogoshi, *J. Am. Chem. Soc., 115* (1993) 2049–2051. (h) Y. Kuroda, M. Ito, T. Sera and H. Ogoshi, *J. Am. Chem. Soc., 115* (1993) 7003–7004. (i) A. Osuka and K. Maruyama, *Tetrahedron, 45* (1989) 4815–4829.

[10] (a) H.L. Anderson, C.A. Hunter, N.M. Meah and J.K.M. Sanders, *J. Am. Chem. Soc., 112* (1990) 5780–5789. (b) R.J. Harrison, B. Pearce, G.S. Beddard, J.A. Cowan and J.K.M. Sanders, *Chem. Phys., 116* (1987) 429–448.

[11] (a) G.R. Seely, *J. Phys. Chem., 76* (1972) 172–180. (b) B.G. Maiya and V. Krishnan, *J. Phys. Chem., 89* (1985) 5225–5235, and references cited therein. (c) G.R. Seely, *Tetrahedron, 45* (1989) 4729–4736. (d) F. D'Souza and V. Krishnan, *Photochem. Photobiol., 51* (1990) 285–291. (e) D. Gust, T.A. Moore, D.K. Luttrull, G.R. Seely, E. Bittersmann, R.B. Bensasson, M. Rougée, E.J. Land, F.C. De Schriver and M. Van der Auweraer, *Photochem. Photobiol., 51* (1990) 419–426. (f) F. D'Souza and V. Krishnan, *Photochem. Photobiol., 56* (1992) 145–156. (g) C. Turró, C.K. Chang, G.E. Leroi, R.I. Cukier and D.G. Nocera, *J. Am. Chem. Soc., 114* (1992) 4013–4015. (h) M. Sirish and B.G. Maiya, *J. Photochem. Photobiol. A: Chem., 77* (1994) 189–200.

[12] (a) M.A. Fox, *Acc. Chem. Res., 25* (1992) 569–574, and references cited therein. (b) P. Castán, J.M. Ribó and F.R. Trull, *React. Polym., 9* (1988) 237–247. (c) J.M. Ribó, M.L. Sesé and F.R. Trull, *React. Polym., 10* (1989) 239–258. (d) S. Nonell, M.L. Sesé, D.O. Mártire, S.E. Braslavsky and F.R. Trull, *Photochem. Photobiol., 53* (1991) 185–193.

[13] C. Colominas, L. Eixarch, P. Fors, K. Lang, S. Nonell, J. Teixidó and F.R. Trull, *J. Chem. Soc., Faraday Trans. 2*, submitted for publication.

[14] (a) J.A. Riddick and W.B. Bunger, in A. Weissberger (ed.), *Techniques of Chemistry. Volume II. Organic Solvents*, Wiley Interscience, New York, 1970. (b) D.D. Perrin, D.R. Perrin and W.L.F. Armarego, *Purification of Laboratory Chemicals*, Pergamon, Oxford, 1980.

[15] Y. Lion, M. Delmelle and A. Van de Vorst, *Nature, 263* (1976) 442–443.

[16] (a) S.E. Braslavsky and K. Heihoff, in J.C. Scaiano (ed.), *CRC Handbook of Organic Photochemistry*, Vol. 1, CRC Press, Boca Raton, FL, 1989, Chapter 14. (b) M. Terazima and T. Azumi, *Bull. Chem. Soc. Jpn., 63* (1990) 741–745. (c) S.E. Braslavsky and G.E. Heibel, *Chem. Rev., 92* (1992) 1381–1410. (d) Ph. Van Haver, L. Viaene, M. Van der Auweraer and F.C. De Schryver, *J. Photochem. Photobiol. A: Chem., 63* (1992) 265–277.

[17] (a) G. Valduga, S. Nonell, E. Reddi, G. Jori and S.E. Braslavsky, *Photochem. Photobiol., 48* (1988) 1–5. (b) S. Nonell, M. González and F.R. Trull, *Afinidad, 448* (1993) 445–450.

[18] (a) M.D. Bentley and M.J.S. Dewar, *Tetrahedron Lett., 50* (1967) 5043–5047. (b) G.M. Sanders, M. van Dijk, A. van Veldhuizen and H.C. van der Plas, *J. Chem. Soc., Chem. Commun.*, (1986) 1311–1313. (c) G.M. Sanders, M. van Dijk, A. van Veldhuizen and H.C. van der Plas, *J. Org. Chem., 53* (1988) 5273–5281. (d) C.A. Hunter and J.K.M. Sanders, *J. Am. Chem. Soc., 112* (1990) 5525–5534.

[19] (a) H.A. Garrera, J.J. Cosa and C.M. Previtali, *J. Photochem. Photobiol. A: Chem., 56* (1991) 267–274. (b) H.A. Montejano, V. Avila, H.A. Garrera and C.M. Previtali, *J. Photochem. Photobiol. A: Chem., 72* (1993) 117–122.

[20] J.R. Lackowicz, *Principles of Fluorescence Spectroscopy*, Plenum, New York, 1986, pp. 257–301.

[21] R.H. Felton, in D. Dolphin (ed.), *The Porphyrins*, Vol. V, Academic Press, New York, 1978, Part C, pp. 53–125.

[22] A.J. Bard and R.L. Faulkner, *Electrochemical Methods: Fundamentals and Applications*, Wiley, New York, 1980, p. 224.

[23] J.R. Darwent, P. Douglas, A. Harriman, G. Porter and M.-C. Richoux, *Coord. Chem. Rev., 44* (1982) 83–126.
[24] G.J. Kavarnos and N.J. Turro, *Chem. Rev., 86* (1986) 401–449.
[25] (a) S.J. Silvers and A. Tulinsky, *J. Am. Chem. Soc., 89* (1967) 3331–3337. (b) M.J.S. Dewar and W. Thiel, *J. Am. Chem. Soc., 99* (1977) 4907–4917.
[26] A. Weller, *Z. Phys. Chem. Neue Folge, 133* (1982) 93–98.
[27] M.R. Wasielewski, D.G. Johnson, M.P. Niemczyk, G.L. Gaines, M.P. O'Neil and W.A. Svec, in J.R. Bolton, N. Mataga and G. McLendon (eds.), *Electron Transfer in Inorganic, Organic, and Biological Systems*, Advances in Chemistry Series 228, ACS, Washington, 1991, pp. 133–148.
[28] R.A. Marcus, *Int. J. Chem. Kinet., 13* (1981) 865–872.
[29] (a) H. Heitele and M.E. Michel-Beyerle, *J. Am. Chem. Soc., 107* (1985) 8286–8288. (b) N.S. Hush, *Coord. Chem. Rev., 64* (1985) 135–157.
[30] A. Gilbert and J. Baggott, *Essentials of Molecular Photochemistry*, Blackwell Scientific Publications, Oxford, 1981, p. 178.
[31] J.P. Keene, D. Kessel, E.J. Land, R.W. Redmond and T.G. Truscott, *Photochem. Photobiol., 43* (1986) 117–120.